ORIGINAL RESEARCH PAPER
Pages: 158-181

Direction of Arrival Estimation of Coherent Sources in Uniform Circular Arrays Using an Iterative Method

Y. Eghbali, M. Ferdosizadeh, and P. Soleimani Salek
Department of Electrical Engineering, Shahed University, Tehran, Iran
mah.ferdosi@gmail.com, yasoubeghbali@gmail.com, p.soleimani12@yahoo.com
Corresponding author: mah.ferdosi@gmail.com

DOI:10.22070/JCE.2022.16895.1223

***Abstract*- In this paper, an iterative algorithm for direction of arrival (DoA) estimation of coherent sources with a uniform circular array (UCA) is proposed. There is an additional error in the DoA estimation of signals after mapping UCA to virtual uniform linear array (VULA), due to approximation of beamspace transformation. This error depends on the direction of emitters. In the proposed algorithm, the dominant term of error is reduced using two beamformers. Then, the DoA of coherent sources is estimated by construction of Toeplitz covariance matrix and using the MUSIC algorithm. The processes of DoA estimation and reduction of the approximation error are done iteratively. Also, an analytical expression is derived for the approximation of bias for DoA estimation of coherent sources. Simulation results show that the proposed algorithm has a better performance in comparison to the conventional methods.**

***Index Terms*-** Direction of arrival (DoA) estimation, coherent sources, uniform circular array (UCA), beamspace transformation (BT), bias reduction.

I. INTRODUCTION

Direction of arrival (DoA) estimation is one of the most important research areas in array signal processing which has so many applications in localization, tracking, surveillance, and navigation [1-4]. Sub-space based DoA estimation methods, such as MUSIC [5] and ESPRIT [6] which are based on the Eigen structure of the received vector covariance matrix are the most powerful methods for DoA estimation. However, these methods are unable to estimate the DoA of coherent sources. At the presence of coherent sources, the source covariance matrix is not full-ranked (is rank deficient). Some modified methods have been proposed for DoA estimation of coherent sources in uniform linear arrays (ULAs) such as: Spatial Smoothing (SS) [7-10], reconstruction of the Toeplitz structure of covariance matrix

Manuscript received 15-March-2021 and revised 11-May-2021, *P-ISSN: 2322-4088*
Accepted on 13- June-2021 *E-ISSN:2322-3936*

[11-12], Spatial Differencing (SD) [13], $M\ell_{1,2}$-MUSIC [14], and Beamspace matrix reconstruction [15].

Uniform circular arrays (UCAs) have some advantages over ULAs such as uniform estimation error over [0, 360]°. But the steering matrix of the UCA is not Vandermonde [16]. By using some preprocessing operations, the UCA can be mapped to a virtual uniform linear array (VULA) with Vandermonde structured steering vectors. Some examples of these mappings are Array Interpolation Techniques (AIT) [17-18], Beamspace Transform (BT) [19-20] and Manifold Separation Technique (MST) [21-22]. In these methods, the steering vectors of UCA are mapped to new steering vectors with Vandermonde structure which is called VULA.

AIT uses a transformation matrix to map the steering vectors of UCA in some predefined and quantized angles (called grid points) to the corresponding steering vectors of a ULA. By application of this transformation, the power of noise vector is increased, because the transform matrix is usually ill-conditioned [23]. In addition to this drawback, AIT leads to a considerable error, when the true DoAs are not on the quantized grid points.

The Vanderomonde structure of ULA steering vectors makes it possible to use root-MUSIC algorithm, which has a better performance in comparison to the MUSIC method. Since the steering vector of UCA is not Vandermonde structured, root-MUSIC algorithm can not be applied directly. In [24], MST was proposed to convert the steering vector of UCA, such that the root-MUSIC algorithm can be applied. Since the root-MUSIC algorithm is unable to find the DoAs of correlated sources, then the MST is not applicable for this purpose.

Based on the above discussion, among the aforementioned transforms, BT is a more suitable transformation, which does not change the power of noise and as we will propose in this paper, it can be used for DoA estimation of coherent sources. Using BT leads to the reduction of the complexity of DoA estimation as well as performance improvement in comparison to the conventional element-space methods [20]. But the mapping from element domain to beam domain produces additional errors which can relieve these advantages.

Similar to ULAs, in UCAs, conventional subspace-based methods such as MUSIC are unable to estimate the DoA of coherent sources. SS algorithm [25], Modified UCA-ESPRIT [26], MODE-TOEP algorithm [26] and modified MUSIC algorithm [27] are some methods which have been proposed for DoA estimation of coherent sources in circular arrays. Among these methods, the SS algorithm is more complex due to use of sub-arrays, while Modified UCA-ESPRIT has lower computational complexities. Furthermore, the last two algorithms can detect more coherent signals under certain conditions.

The accuracy of the above-mentioned algorithms is degraded due to the residual error caused by BT, when it is applied to UCAs. In BT transformation, phase mode excitation principle is used to convert the steering vectors of UCA to the steering vectors of a VULA. The approximation in this conversion leads to residual errors, which introduces bias or additional error variance in DoA estimation [20]. Since

the resulted error depends on the DoAs of signals, there is not a direct method to remove the residual error and iterative methods must be used in which estimation of DoAs and removal of residual errors are done iteratively.

In [20], it has been shown that the residual error of BT for noncoherent sources can be reduced iteratively, but there is no proposed method for reduction of the residual error of BT for coherent sources. In this paper, an Iterative Mode Toeplitz and Bias Removal (IMTBR) method for DoA estimation of coherent sources in UCA has been proposed. At the first step of IMTBR, conventional BT is applied to the UCA received vector and Toeplitz covariance matrix is constructed. Then, the initial estimated DoAs are obtained by application of MUSIC algorithm to the Toeplitz structured covariance matrix. This initial estimation has error due to the noise and bias caused by BT. At the second step, the error caused by BT is reduced using the beamformers presented in [20] and the first step is repeated. The processes of DoA estimation using Toeplitz structured covariance matrix and removal of the dominant term of BT bias are repeated iteratively. Also, an analytical expression for the first approximation of the bias in DoA estimation of the coherent sources is obtained.

The paper is structured as follows: In section II, the system model of DoA estimation in circular arrays is presented. In section III, phase mode excitation principle is described briefly. In section IV, BT is defined. The proposed iterative algorithm for DoA estimation of coherent sources is introduced in section V. A first-order approximation of the bias in DoA estimation of coherent sources is obtained in section VI. Computational complexity of the proposed method is calculated in section VII. Simulation results are shown in section VIII. Finally, section XI concludes the paper.

Notations: Scalars, matrices and vectors are represented by normal letters, boldface uppercase and boldface lowercase letters, respectively. $\mathbb{C}$ is the set of complex numbers, $\Re$ represents the real part operation, and diag{.} denotes a diagonal matrix. $\mathbf{I}_N$ and $\tilde{\mathbf{I}}_N$ denote $N \times N$ identity and exchange matrices, respectively. $\odot$ is HadamardSchur (element by element) product and $\mathcal{O}$ denotes complexity order. $(.)^T$, $(.)^*$, $(.)^H$, $(.)^{-1}$, $(.)^\dagger$ stand for the transpose, conjugate, conjugate transpose, inverse, and pseudo-inverse, respectively.

II. SYSTEM MODEL

It is assumed that there are K narrowband sources, and an ideal UCA consists of $N(N > K)$ identical and omnidirectional antennas located uniformly on a circle with radius r. The n-th antenna has been located on a circle of radius r and in direction of $\gamma_n = \frac{2\pi n}{N}(n = 0,1,\ldots..., N-1)$. The Cartesian coordinate of the n-th antenna is $\left(r\cos\left(\frac{2\pi n}{N}\right), r\sin\left(\frac{2\pi n}{N}\right), 0\right)$. Assuming that coupling effects between different antennas are zero, the output vector, $\mathrm{x(t)} \in \mathbb{C}^{N\times 1}$, at discrete time index t (the continuous

equivalent time is $t\Delta t$, where Δt is sampling period) can be represented as

$$\mathbf{x}(t) = \mathbf{A}(\phi)\mathbf{s}(t) + \mathbf{n}(t) \quad (1)$$

where $s(t) = [s_1(t), s_2(t), \dots, s_k(t)]^T \in \mathbb{C}^{k\times 1}$ is the source signal vector and $n(t) = [n_1(t), n_2(t), \dots, n_k(t)]^T \in \mathbb{C}^{N\times 1}$ denotes the noise vector. The noise of antennas is assumed to be spatially and temporally white complex Gaussian random process with zero mean and similar variance of σ^2 . Also, $A(\phi) \in \mathbb{C}^{N\times k}$ is the steering matrix which is defined by [20]

$$\mathbf{A}(\phi) = [\mathbf{a}(\phi_1), \mathbf{a}(\phi_2), \dots, \mathbf{a}(\phi_K)] \quad (2)$$

where

$$\mathbf{a}(\phi_k) = \left[e^{\frac{2j\pi fr}{c}\cos(\phi_k - \gamma_0)}, e^{\frac{2j\pi fr}{c}\cos(\phi_k - \gamma_1)}, \dots, e^{\frac{2j\pi fr}{c}\cos(\phi_k - \gamma_{N-1})} \right]^T \quad (3)$$

is the k -th column of $\mathbf{A}(\phi)$ and ϕ_k is the angle of arrival of the k -th source as shown in Fig. 1. It has been assumed that the sources and antennas are located at the same plane.

If ζ is defined by $2\pi fr / c$, then $\mathbf{a}(\phi_k)$ can be rewritten as

$$\mathbf{a}(\phi_k) = \left[e^{j\zeta\cos(\phi_k - \gamma_0)}, e^{j\zeta\cos(\phi_k - \gamma_1)}, \dots, e^{j\zeta\cos(\phi_k - \gamma_{N-1})} \right]^T \quad (4)$$

It is clearly obvious that the steering matrix of UCA is not Vandermonde structured, thus it is not possible to use properties of Vandermonde matrices to estimate DoAs. Therefore, preprocessing methods such as BT, which is based on the phase mode excitation principle, are used to map the steering matrix of UCA array to a matrix with Vandermonde structure corresponding to a VULA.

III. PHASE-MODE EXCITATION PRINCIPLE

The ideal configuration for applying phase-mode excitation principle is to consider a continuous array that is not practically implementable [20]. Thus, we review the phase-mode excitation principle in continuous circular array and then it is investigated in discrete case with uniform placement of N elements in circular configuration. DoA problem is dual of beamforming. Thus, the principle of mode excitation has been described based on beamforming in [20], which has been briefly described in the following subsections.

A. Continuous Circular Aperture

Consider a continuous circular array that has been excited by the excitation function $\omega(\gamma)$, $0 < \gamma \le 2\pi$. It means that the point mounted on the array in angular position γ is excited by the voltage $\omega(\gamma)$. Any excitation function in continuous circular aperture is periodic with period of 2π ,

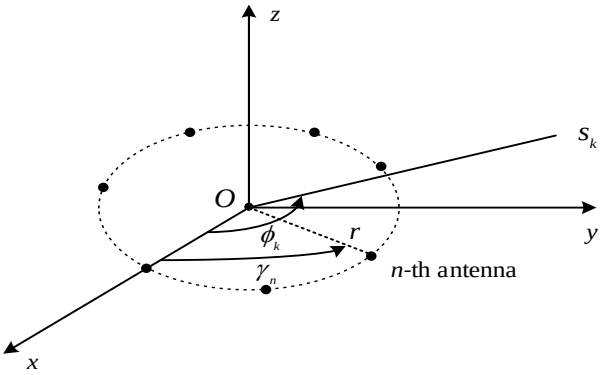

Fig. 1. UCA with N antenna.

and it can be shown by a Fourier series. Using Fourier series representation, the excitation function $\omega(\gamma)$ can be expressed as $\omega(\gamma)=\sum_{m=-\infty}^{\infty} c_m e^{jm\gamma}$, where the m-th phase mode $\omega_m(\gamma)=e^{jm\gamma}$ is a spatial harmonic to excite the array, and its corresponding coefficient is c_m. In [20], the normalized far-field pattern resulted from the m-th phase-mode is calculated as (5), which is shown in the next page.

$$f_m^c(\phi)=\frac{1}{2\pi}\int_0^{2\pi}\omega_m(\gamma)e^{j\zeta\cos(\phi-\gamma)}d\gamma \tag{5}$$

The superscript c stands for continuous case. This pattern can be expressed in terms of Bessel function [20]:

$$f_m^c(\phi)=j^m J_m(\zeta)e^{jm\phi} \tag{6}$$

where $J_m(\zeta)$ is the Bessel function of the first kind of order m. The term $e^{jm\phi}$ in (6) shows that the far filed pattern has the same variation with ϕ as the m-th phase mode excitation, $\omega_m(\gamma)=e^{jm\phi}$. Therefore, different excitations with proper coefficients, c_m, can be used to produce any far-field pattern in continuous circular arrays. Due to the amplitude and the elevation dependence of the far-field pattern via the Bessel function, only a finite number of modes can be excited by a given circular aperture. To calculate the highest excitable order mode (M), it should be considered that the amplitude of the m-th excited mode is $J_m(\zeta)$ and the value of the Bessel function is negligible when the arguments of this function exceeds its order i.e., $\zeta > m$. Thus, the highest excitable mode, $J_m(\zeta)$, is the highest integer that $M \le \zeta = 2\pi fr/c$ and excitable modes are $m \in [-M, M]$.

B. Discrete Uniform Circular Array

In a discrete version of circular array (UCA), a limited number of antennas are uniformly placed on a circle (at angular positions $\gamma_0, \gamma_1, ..., \gamma_{N-1}$).The normalized beamforming weight vector that excites the array with phase mode $m \in [-M, M]$ changes to The superscript s stands for sampled or

$$\mathbf{w}_m = \frac{1}{N}\left[e^{jm\gamma_0}, e^{jm\gamma_1}, \ldots, e^{jm\gamma_{N-1}}\right]^H = \frac{1}{N}\left[1, e^{j\frac{2\pi m}{N}}, \ldots, e^{j\frac{2\pi m(N-1)}{N}}\right]^H \quad (7)$$

The resulting array pattern is

$$f_m^s(\phi) = \mathbf{w}_m^H \mathbf{a}(\phi) = \frac{1}{N}\sum_{n=0}^{N-1} e^{jm\gamma_n} e^{j\zeta\cos(\phi-\gamma_n)} \quad (8)$$

discrete array. In [20], it has been shown that this pattern for $|m| \le M$ can be written as

$$f_m^s(\phi) = j^m J_m(\zeta) e^{jm\phi} + \sum_{q=1}^{\infty}\left(j^g J_g(\zeta) e^{-jg\phi} + j^h J_h(\zeta) e^{jh\phi}\right) \quad (9)$$

where $h = Nq + m$ and $g = Nq - m$. In (9), the principal term (the first term) is equal to the far-field pattern of continuous aperture as shown in (6). The two other terms, which are called the residual terms are resulted from sampling of continuous aperture. Thus, the residual error term is defined by

$$\epsilon_m(\phi) = \sum_{q=1}^{\infty}\left(j^g J_g(\zeta) e^{-jg\phi} + j^h J_h(\zeta) e^{jh\phi}\right) \quad (10)$$

and (9) can be rewritten as

$$f_m^s(\phi) - j^m J_m(\zeta) e^{jm\phi} + \epsilon_m(\phi) \quad (11)$$

In order to obtain the ideal case performance, the residual term must be minimized. In [20], it has been shown that if $N > 2m$, then the principal term in (11) is dominant one. Since the highest excited mode is M, then the number of elements, must be chosen such that $N > 2m$. This result looks like the Nyquist sampling criterion in which M defines the maximum spatial component for array excitation.

Although the above limitation on the number of elements guarantees that the principle term is dominant, but the residual term may still be considerable. To show this phenomenon, we have calculated the main term and residual error terms for a UCA with $M = 3$ excitable modes ($f = 1GH$, $r = Mc/2\pi f$). Table I shows the values of different terms of (11), for $m = -3, -2, -1, 0, 1, 2, 3$ in case of $\phi = 50^\circ$.

It is observed that the main term is more significant in comparison to the residual terms. Also, the residual error term for $q = 1$ is considerable. Therefore, we only consider the residual errors resulted from $q = 1$. Thus, the resulting array pattern is approximated by

$$f_m^s(\phi) \approx j^m J_m(\zeta) e^{jm\phi} + j^{N-m} J_{N-m}(\zeta) e^{-j(N-m)\phi} + j^{N+m} J_{N+m}(\zeta) e^{j(N+m)\phi} \quad (12)$$

If the number of antennas of UCA, N, is chosen such that the residual terms are negligible for mode orders $|m| \le M$, the array patterns for discrete aperture UCA are identical to continuous circular aperture. Then the residual term can be ignored and we can use the following approximation

$$f_m^s(\phi) \approx j^m J_m(\zeta) e^{jm\phi} \quad (13)$$

Table I. The values of different terms of array pattern at $\phi = 50^{\circ}$

m	**Main term**	**Error term** $(q=1)$	**Error term** $(q=2)$	**Error term** $(q=3)$
–3	3.0906×10^{-1}	4.3028×10^{-2}	2.6591×10^{-8}	8.8116×10^{-17}
–2	4.8609×10^{-1}	1.1396×10^{-2}	2.8800×10^{-8}	6.0348×10^{-18}
–1	3.3906×10^{-1}	2.5340×10^{-2}	2.9306×10^{-8}	3.9594×10^{-19}
0	2.6005×10^{-1}	7.5600×10^{-2}	9.5466×10^{-8}	2.4793×10^{-20}
1	3.3906×10^{-1}	2.5340×10^{-2}	2.9306×10^{-8}	3.9594×10^{-19}
2	4.8609×10^{-1}	1.1396×10^{-2}	2.8800×10^{-8}	6.0348×10^{-18}
3	3.0906×10^{-1}	4.3028×10^{-2}	2.6591×10^{-8}	8.8116×10^{-17}

IV. BEAMSPACE TRANSFORM

The BT maps the steering vectors of UCA into the steering vectors of a VULA with Vandermonde structure. This transform makes it possible to apply some widely used and efficient methods for UCA that were originally designed for ULA, such as root-MUSIC, ESPRIT, and SS [20].

In [20], the matrix $\mathbf{F}_e^H$ has been used to transform element space to beamspace. The UCA steering vector of (4) is mapped to the VULA array through this beamformer, which is defined by

$$\mathbf{F}_e^H = \mathbf{C}_v \mathbf{V}^H \tag{14}$$

where $\mathbf{C}_v = \text{diag}\left\{ j^{-M}, \ldots, j^{-1}, j^0, j^{-1}, \ldots, j^{-M} \right\}$ and $\mathbf{V} = \sqrt{N}[\mathbf{w}_{-M}, \ldots, \mathbf{w}_0, \ldots, \mathbf{w}_M]$. The columns of $\mathbf{V}$, $(\sqrt{N}\mathbf{w}_m, m = -M, -M+1, ..., M-1, M)$ are defined by (7). Applying beamformer $\mathbf{F}_e^H$ to the UCA steering vector, based on (9) and (13), the new steering vector is obtained as

$$\begin{aligned} \mathbf{a}_e(\phi_k) &= \mathbf{F}_e^H \mathbf{a}(\phi_k) = \mathbf{C}_v \mathbf{V}^H \mathbf{a}(\phi_k) = \sqrt{N}\mathbf{C}_v [\mathbf{w}_{-M}, ..., \mathbf{w}_0, ..., \mathbf{w}_M]^H \mathbf{a}(\phi_k) \\ &= \sqrt{N}\mathbf{C}_v [\mathbf{w}_{-M}^H \mathbf{a}(\phi_k), ..., \mathbf{w}_0^H \mathbf{a}(\phi_k), ..., \mathbf{w}_M^H \mathbf{a}(\phi_k)]^T \\ &\approx \sqrt{N}\mathbf{C}_v [\, j^{-M} J_{-M}(\zeta) e^{-jM\phi_k}, ..., j^0 J_0(\zeta), ..., j^M J_M(\zeta) e^{jM\phi_k}\,]^T \end{aligned} \tag{15}$$

Using the property $J_{-m}(\zeta) = (-1)^m J_{|m|}(\zeta)$, (15) can be rewritten as

$$\begin{aligned} \mathbf{a}_e(\phi_k) &\approx \sqrt{N}\mathbf{C}_v \text{diag}\left\{ (-j)^{-M} J_M(\zeta) e^{-jM\phi_k}, ..., J_0(\zeta), ..., j^M J_M(\zeta) e^{-jM\phi_k} \right\} \\ &= \sqrt{N}\,\text{diag}\left\{ J_M(\zeta) e^{-jM\phi_k}, ..., J_0(\zeta), ..., J_M(\zeta) e^{-jM\phi_k} \right\} = \sqrt{N}\mathbf{J}_\zeta \tilde{\mathbf{a}}(\phi_k) \end{aligned} \tag{16}$$

where

$$\tilde{\mathbf{a}}(\phi_k) = \left[e^{-jM\phi_k}, \ldots, e^{-j\phi_k}, e^{j0}, e^{j\phi_k}, \ldots, e^{jM\phi_k} \right]^T \tag{17}$$

is the steering vector of VULA with Vandemonde structure and

$$\mathbf{J}_\zeta = \text{diag}\left\{ J_M(\zeta), \ldots, J_1(\zeta), J_0(\zeta), J_1(\zeta), \ldots, J_M(\zeta) \right\} \tag{18}$$

The obtained new steering vector in (16) is an approximation and to make it more accurate, two

additional terms are also taken into account in [20]. Thus, a more accurate representation of $\mathbf{a}_e(\phi_k)$ is as follows

$$\mathbf{a}_e(\phi_k) = \sqrt{N}\mathbf{J}_\zeta\left(\tilde{\mathbf{a}}(\phi_k) + \Delta\mathbf{d}_1(\phi_k) + \Delta\mathbf{d}_2(\phi_k)\right) \tag{19}$$

where $\Delta d_1(\phi) = J_\zeta^{-1} C_v \in^{(1)}(\phi_k)$ and $\in^{(1)}(\phi_k) = \in_2^{(1)}(\phi_k) + \in_2^{(1)}(\phi_k)$ such that $\in_1^{(1)}(\phi_k)$ and $\in_2^{(1)}(\phi_k)$ are defined as follows:

$$\boldsymbol{\epsilon}_1^{(1)}(\phi_k) = \begin{bmatrix} j^{(N+M)} J_{N+M}(\zeta) e^{-j(N+M)\phi_k} \\ j^{(N+M-1)} J_{N+M-1}(\zeta) e^{-j(N+M-1)\phi_k} \\ \vdots \\ j^{N} J_{N}(\zeta) e^{-j(N)\phi_k} \\ \vdots \\ j^{(N-M+1)} J_{N-M+1}(\zeta) e^{-j(N-M+1)\phi_k} \\ j^{(N-M)} J_{N-M}(\zeta) e^{-j(N-M)\phi_k} \end{bmatrix} \tag{20}$$

$$\boldsymbol{\epsilon}_2^{(1)}(\phi_k) = \begin{bmatrix} j^{(N-M)} J_{N-M}(\zeta) e^{j(N-M)\phi_k} \\ j^{(N-M+1)} J_{N-M+1}(\zeta) e^{j(N-M+1)\phi_k} \\ \vdots \\ j^{N} J_{N}(\zeta) e^{j(N)\phi_k} \\ \vdots \\ j^{(N+M-1)} J_{N+M-1}(\zeta) e^{j(N+M-1)\phi_k} \\ j^{(N+M)} J_{N+M}(\zeta) e^{j(N+M)\phi_k} \end{bmatrix} \tag{21}$$

Since $\Delta\mathbf{d}_2(\phi_k)$ includes high order error terms in (19) and considerably small compared to $\Delta\mathbf{d}_1(\phi_k)$, thus equation (19) can be approximated as

$$\mathbf{a}_e(\phi_k) \approx \sqrt{N}\mathbf{J}_\zeta\left(\tilde{\mathbf{a}}(\phi_k) + \Delta\mathbf{d}_1(\phi_k)\right) \tag{22}$$

V. IMTBR ALGORITHM FOR DOA ESTIMATION OF COHERENT SOURCES

In [20], a modified BT, based on phase-mode excitation principle, is introduced. This transform performs mapping from element-space to beamspace domain by taking into account the error caused by the transform. The authors proposed an iterative technique to remove the bias introduced by the BT in the DoA estimation. In addition, they have derived an expression, which approximates the bias in DoA estimation caused by BT transform.

In this section, we present an algorithm using two beamformers, $\mathbf{F}_{e_1}^H$ and $\mathbf{F}_{e_2}^H$, which are introduced

in [20] to improve the accuracy of DoA estimation of coherent sources. Applying the BT of (14) to the output vector of the array, $\mathbf{x}(t)$, the new vector, $\mathbf{y}(t)$, can be obtained as

$$\begin{aligned}\mathbf{y}(t)&=\mathbf{F}_e^H\mathbf{x}(t)=\mathbf{F}_e^H\mathbf{A}\mathbf{s}(t)+\mathbf{F}_e^H\mathbf{n}(t)=\sqrt{N}\left(\mathbf{J}_\zeta\tilde{\mathbf{A}}(\phi)+\mathbf{J}_\zeta\boldsymbol{\Delta}\mathbf{d}_1(\phi)\right)\mathbf{s}(t)+\mathbf{F}_e^H\mathbf{n}(t)\\&=\sqrt{N}\left(\mathbf{J}_\zeta\tilde{\mathbf{A}}(\phi)+\mathbf{C}_v\left(\boldsymbol{\epsilon}_1^{(1)}(\phi)+\boldsymbol{\epsilon}_2^{(1)}(\phi)\right)\right)\mathbf{s}(t)+\mathbf{F}_e^H\mathbf{n}(t)\end{aligned} \tag{23}$$

where $\tilde{\mathbf{A}}(\phi)=\left[\tilde{\mathbf{a}}(\phi_1),\tilde{\mathbf{a}}(\phi_2),...,\tilde{\mathbf{a}}(\phi_K)\right]$ is the VULA steering matrix, $\boldsymbol{\Delta}\mathbf{d}_1(\phi)=[\boldsymbol{\Delta}\mathbf{d}(\phi_1),\boldsymbol{\Delta}\mathbf{d}(\phi_2),...,\boldsymbol{\Delta}\mathbf{d}(\phi_K)]$, $\in_1^{(1)}(\phi)\left[\in_1^{(1)}(\phi_1),\in_1^{(1)}(\phi_2),...\in_1^{(1)}(\phi_k)\right]$ and $\boldsymbol{\epsilon}_2^{(1)}(\phi)=\left[\boldsymbol{\epsilon}_2^{(1)}(\phi_1),\boldsymbol{\epsilon}_2^{(1)}(\phi_2),...,\boldsymbol{\epsilon}_1^{(1)}(\phi_K)\right]$.

In order to improve the accuracy of DoA estimation of coherent sources in UCA, we use two beamformers which are presented in [20]:

$$\mathbf{F}_{e_1}=\sqrt{N}\hat{\mathbf{A}}^{\dagger}[\boldsymbol{\epsilon}_1^{(1)}(\phi)]^H\mathbf{C}_v^H \tag{24}$$

$$\mathbf{F}_{e_2}=\sqrt{N}\hat{\mathbf{A}}^{\dagger}[\boldsymbol{\epsilon}_2^{(1)}(\phi)]^H\mathbf{C}_v^H \tag{25}$$

where $\hat{\mathbf{A}}^{\dagger}=\mathbf{A}(\hat{\phi})\left(\mathbf{A}^H(\hat{\phi})\mathbf{A}(\hat{\phi})\right)^{-1}$. Applying these two beamformers to the array output vector, two output vectors $\tilde{\mathbf{y}}_1(t)$ and $\tilde{\mathbf{y}}_2(t)$ are obtained as

$$\tilde{\mathbf{y}}_1(t)=\mathbf{F}_{e_1}^H\mathbf{x}(t)=\left(\sqrt{N}\mathbf{C}_v\boldsymbol{\epsilon}_1^{(1)}(\phi)\right)\mathbf{s}(t)+\mathbf{F}_{e_1}^H\mathbf{n}(t) \tag{26}$$

$$\tilde{\mathbf{y}}_2(t)=\mathbf{F}_{e_2}^H\mathbf{x}(t)=\left(\sqrt{N}\mathbf{C}_v\boldsymbol{\epsilon}_2^{(1)}(\phi)\right)\mathbf{s}(t)+\mathbf{F}_{e_2}^H\mathbf{n}(t) \tag{27}$$

To eliminate the bias, we have to remove the difference between the beamspace data vector $\mathbf{y}(t)$ and $\tilde{\mathbf{y}}_1(t)+\tilde{\mathbf{y}}_2(t)$ as

$$\hat{\mathbf{y}}(t)=\mathbf{y}(t)-\left(\tilde{\mathbf{y}}_1(t)+\tilde{\mathbf{y}}_2(t)\right)=\left(\mathbf{F}_e^H-\left(\mathbf{F}_{e_1}^H+\mathbf{F}_{e_2}^H\right)\right)\mathbf{x}(t)=\sqrt{N}\mathbf{J}_\zeta\tilde{\mathbf{A}}(\phi)\mathbf{s}(t)+\left(\mathbf{F}_e^H-\left(\mathbf{F}_{e_1}^H+\mathbf{F}_{e_2}^H\right)\right)\mathbf{n}(t) \tag{28}$$

Since $\|\boldsymbol{\epsilon}_1^{(1)}(\phi)\|_2\ll 1$ and $\|\boldsymbol{\epsilon}_2^{(1)}(\phi)\|_2\ll 1$, then $(\mathbf{F}_e^H-\mathbf{F}_{e_1}^H-\mathbf{F}_{e_2}^H)$ is very close to unitary and $(\mathbf{F}_e^H-\mathbf{F}_{e_1}^H-\mathbf{F}_{e_2}^H)(\mathbf{F}_e^H-\mathbf{F}_{e_1}^H-\mathbf{F}_{e_2}^H)^H\approx\mathbf{F}_e^H\mathbf{F}_e=\mathbf{I}_{2M+1}$. Therefore, the statistics of the noise will not be changed considerably.

When the signals are coherent, the source covariance matrix is not full-rank and the MUSIC algorithm is not applicable to estimate the DoAs of coherent signals. Thus, we have to make the source covariance matrix full-rank. This matrix can be obtained by using the MODE-TOEP algorithm which is proposed in [27].

By the multiplication of the beamspace vector, $\mathbf{y}(t)$ in (23), by the matrix $\frac{\mathbf{J}_\zeta^{-1}}{\sqrt{N}}$, the new vector, $\mathbf{z}(t)$, can be obtained as

$$\mathbf{z}(t)=\frac{\mathbf{J}_{\zeta}^{-1}}{\sqrt{N}}\mathbf{y}(t)=\left(\tilde{\mathbf{A}}(\phi)+\Delta\mathbf{d}_1(\phi)\right)\mathbf{s}(t)+\tilde{\mathbf{n}}(t) \tag{29}$$

where $\tilde{\mathbf{n}}(t)=\frac{\mathbf{J}_{\zeta}^{-1}}{\sqrt{N}}\mathbf{F}_e^H\mathbf{n}(t)$. Since the matrix $\mathbf{J}_{\zeta}^{-1}$ is diagonal, then the new noise vector $\tilde{\mathbf{n}}(t)$ is non-uniform, but still uncorrelated. Considering K coherent signals received at array such that $\left(s_k(t)=\rho_k s_1(t), k=2,...,K\right)$ and also the central virtual antenna as the reference, the received signal in the h-th virtual antenna at discrete time index t can be expressed as

$$\begin{aligned} z_h(t)&=\sum_{k=1}^{K}\left(\tilde{a}_h(\phi_k)+\Delta d_{1,h}(\phi_k)\right)s_k(t)+\tilde{n}_h(t)\\ &=s_1(t)\sum_{k=1}^{K}\left(\tilde{a}_h(\phi_k)+\Delta d_{1,h}(\phi_k)\right)\rho_k+\tilde{n}_h(t), h=1,2,...,2M+1 \end{aligned} \tag{30}$$

In (30), $\tilde{a}_h(\phi_k)$, $\Delta d_{1,h}(\phi_k)$, $z_h(t)$ and $\tilde{n}_h(t)$ are the h-th elements of the vectors $\tilde{\mathbf{a}}(\phi_k)$, $\Delta\mathbf{d}_1(\phi_k)$, $\mathbf{z}(t)$ and $\tilde{\mathbf{n}}(t)$, respectively. Also, $s_k(t)$ is the k-th elements of the vector $\mathbf{s}(t)$. For the simplicity, we have considered that the signal of the sources is completely correlated. It means that the absolute value of the correlation coefficient between any pair of the sources is equal to one. The proposed algorithm also works for the cases where the signals are partially correlated.

Spatial correlation between the reference and the h-th virtual antenna can be defined by

$$r(M+1-h)=E\left\{z_{M+1}(t)z_h^*(t)\right\} \tag{31}$$

It is noteworthy that $z_{M+1}(t)$ is the signal of the virtual reference antenna. Also, with some modification, we can rewrite the equation (31) as follows:

$$\begin{aligned} r(M+1-h)&=P\sum_{p=1}^{K}\sum_{q=1}^{K}\rho_p\rho_q^*\tilde{a}_{M+1}(\phi_p)\tilde{a}_h^*(\phi_q)+P\sum_{p=1}^{K}\sum_{q=1}^{K}\rho_p\rho_q^*\left(\tilde{a}_{M+1}(\phi_p)+\Delta d_{1,M+1}(\phi_p)\right)\Delta d_{1,h}^*(\phi_q)\\ &\quad+P\sum_{p=1}^{K}\sum_{q=1}^{K}\rho_p\rho_q^*\Delta d_{1,M+1}(\phi_p)\tilde{a}_h^*(\phi_q)+\tilde{\sigma}^2\delta_{M+1,h}\ , h=1,2,,...,2M+1 \end{aligned} \tag{32}$$

where $P=E\left\{s_1(t)s_1^*(t)\right\}$, $\tilde{\sigma}^2=E\left\{\tilde{n}_{M+1}(t)\tilde{n}_{M+1}^*(t)\right\}$, and $\delta_{M+1,h}$ is Dirac delta function which is equal to one when $h=M+1$, otherwise it is zero. The covariance matrix with Toeplitz structure is defined as follows:

$$\mathbf{R}_c=\begin{bmatrix} r(0) & r(-1) & \cdots & r(-M)\\ r(1) & r(0) & \cdots & r(-M+1)\\ \vdots & \vdots & \ddots & \vdots\\ r(M) & r(M-1) & \cdots & r(0) \end{bmatrix}=\mathbf{G}(\phi)\mathbf{C}\mathbf{G}^H(\phi)+\mathbf{B}(\phi)+\tilde{\sigma}^2\mathbf{I}_{M+1} \tag{33}$$

where $\mathbf{C}=\text{diag}\{c_1,c_2,...,c_K\}$ with $c_k=P\rho_k^*\sum_{p=1}^{K}\rho_p$, $\mathbf{G}(\phi)$ is the steering matrix of a linear array with M antennas which can be expressed as (34).

$$\mathbf{G}(\phi)=\begin{bmatrix} 1 & 1 & \cdots & 1 \\ e^{j\phi_1} & e^{j\phi_2} & \cdots & e^{j\phi_K} \\ \vdots & \vdots & \ddots & \vdots \\ e^{jM\phi_1} & e^{jM\phi_2} & \cdots & e^{jM\phi_K} \end{bmatrix} \tag{34}$$

and $\mathbf{B}(\phi)$ can be defined as

$$\mathbf{B}(\phi)=\begin{bmatrix} b_{M+1,M+1}(\phi) & b_{M+1,M+2}(\phi) & \cdots & b_{M+1,2M+1}(\phi) \\ b_{M+1,M}(\phi) & b_{M+1,M+1}(\phi) & \cdots & b_{M+1,2M}(\phi) \\ \vdots & \vdots & \ddots & \vdots \\ b_{M+1,1}(\phi) & b_{M+1,2}(\phi) & \cdots & b_{M+1,M+1}(\phi) \end{bmatrix} \tag{35}$$

where $b_{M+1,h}(\phi)$ is

$$b_{M+1,h}(\phi)=P\sum_{p=1}^{K}\sum_{q=1}^{K}\rho_p\rho_q^{*}\Delta d_{1,M+1}(\phi_p)\tilde{a}_h^{*}(\phi_q)+P\sum_{p=1}^{K}\sum_{q=1}^{K}\rho_p\rho_q^{*}\left(\tilde{a}_{M+1}(\phi_p)+\Delta d_{1,M+1}(\phi_p)\right)\Delta d_{1,h}^{*}(\phi_q) \tag{36}$$
$$,h=1,2,,...,2M+1$$

As can be seen from (32) and (33), although the powers of the elements of the noise vector, $\tilde{\mathbf{n}}(t)$, are not the same, but the effect of the noise after Toeplitz construction of covariance matrix is appeared as $\tilde{\sigma}^2\mathbf{I}_{M+1}$. It means that the power of noise is distributed uniformly among the components of VULA. Equation (33) has the form of the autocorrelation matrix in DoA estimation methods except the term $\mathbf{B}(\phi)$ that must be eliminated. In the first step of the proposed algorithm, by applying the BT transform to the output vector of the array, the beamspace vector, $\mathbf{y}(t)$, can be derived. Then, $\mathbf{y}(t)$ is multiplied by $\frac{\mathbf{J}_{\zeta}^{-1}}{\sqrt{N}}$ to generate the new vector $\mathbf{z}(t)$. In practice the covariance matrix, $\mathbf{R}_c$, is unavailable and it can be estimated from L snapshots of the received signal vector as follows:

$$\mathbf{R}_c=\begin{bmatrix} \hat{r}(0) & \hat{r}(-1) & \cdots & \hat{r}(-M) \\ \hat{r}(1) & \hat{r}(0) & \cdots & \hat{r}(-M+1) \\ \vdots & \vdots & \ddots & \vdots \\ \hat{r}(M) & \hat{r}(M-1) & \cdots & \hat{r}(0) \end{bmatrix} \tag{37}$$

where $\hat{r}(M+1-h)=\frac{1}{L}\sum_{t=1}^{L}z_{M+1}(t)z_h^{*}(t)$. DoAs are estimated using the MUSIC or root-MUSIC algorithm while neglecting the effect of $\mathbf{B}(\phi)$. In the next step, using the estimated DoAs, ϕ, we calculate $\epsilon_1^{(1)}(\phi)$ and $\epsilon_2^{(1)}(\phi)$ using (20) and (21), and $\mathbf{F}_{e_1}$ and $\mathbf{F}_{e_2}$ are generated using (24) and (25). Then $\tilde{\mathbf{y}}_1(t)=\mathbf{F}_{e_1}^{H}\mathbf{x}(t)$ and $\tilde{\mathbf{y}}_2(t)=\mathbf{F}_{e_2}^{H}\mathbf{x}(t)$ are calculated using (26) and (27). $\hat{\mathbf{y}}(t)$ will be derived after subtracting $\tilde{\mathbf{y}}_1(t)+\tilde{\mathbf{y}}_2(t)$ from $\mathbf{y}(t)$. Using $\hat{\mathbf{y}}(t)$, we can estimate the new $\hat{\mathbf{R}}_c$. In this procedure,

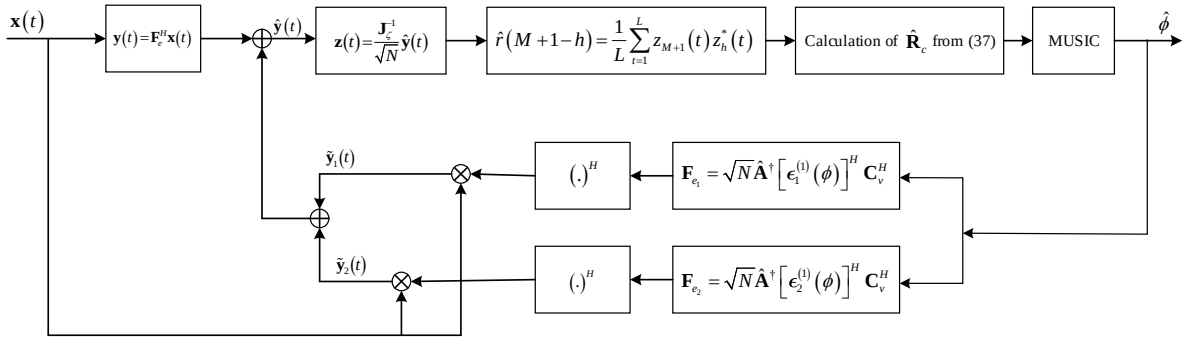

Fig. 2. Block diagram of the proposed IMTBR algorithm.

by repeating the aforementioned steps, the effect of $\mathbf{B}(\phi)$ will be eliminated and we can have a more accurate estimation of DoAs. The proposed method is terminated if $\| \hat{\phi}^{(i)} - \hat{\phi}^{(i-1)} \|_2 < \tau$ or the maximum number of iterations is reached, where τ is a predefined estimation error and the superscript i stands for the iteration. The proposed IMTBR algorithm is summarized in Algorithm 1.

Fig. 2 demonstrates the block diagram of the proposed algorithm in order to increase the accuracy of coherent sources DoA estimation.

Algorithm 1 Iterative Mode Toeplitz and Bias Removal

Input: $\mathbf{x}(t), t = 1, 2, ..., L$, number of iterations, N_{itr}, and τ.

Output: $\hat{\phi} = \left[\hat{\phi}_1, \hat{\phi}_2, ..., \hat{\phi}_K\right]^T$

Initialization: $i = 0$

Step 1:

a. Apply beamspace transform to the output vector of the array, $\mathbf{x}(t)$, and obtain the initial beamspace vector as $\mathbf{y}(t) = \mathbf{F}_e^H \mathbf{x}(t)$.

b. Multiply the beamspace vector, $\mathbf{y}(t)$, by $\frac{\mathbf{J}_\zeta^{-1}}{\sqrt{N}}$ to yield $\mathbf{z}(t)$ and then estimate the covariance matrix of VULA using L snapshots of $\mathbf{z}(t)$ as (37).

c. Estimate the initial DoAs, $\hat{\phi}^{(0)}$, using the MUSIC or root-MUSIC algorithm.

d. $i = i + 1$

Step 2:

while ($i \leq N_{itr}$) **do**

a. Calculate the $\boldsymbol{\epsilon}_1^{(1)}(\hat{\phi}_k^{(i-1)})$ and $\boldsymbol{\epsilon}_1^{(2)}(\hat{\phi}_k^{(i-1)})$ for $k = 1, 2, ..., K$ using (20) and (21), respectively.

b. Calculate the estimated UCA steering matrix with $\phi^{(i-1)}$ according to (2), and consequently, $\tilde{\mathbf{A}}^\dagger = \mathbf{A}(\hat{\phi})\left(\mathbf{A}^H(\hat{\phi})\mathbf{A}(\hat{\phi})\right)^{-1}$.

---

c. Form the beamformers $\mathbf{F}_{e_1}^H$ and $\mathbf{F}_{e_2}^H$ using (24) and (25), respectively.

d. Calculate the correction vectors, $\tilde{\mathbf{y}}_1(t)=\mathbf{F}_{e_1}^H\mathbf{x}(t)$ and $\tilde{\mathbf{y}}_2(t)=\mathbf{F}_{e_2}^H\mathbf{x}(t)$.

e. Obtain $\hat{\mathbf{y}}(t)=\mathbf{y}(t)-\left(\tilde{\mathbf{y}}_1(t)+\tilde{\mathbf{y}}_2(t)\right)$.

f. Multiply $\hat{\mathbf{y}}(t)$ by $\frac{\mathbf{J}_\zeta^{-1}}{\sqrt{N}}$ to yield $\mathbf{z}(t)$ and then re-estimate the covariance matrix.

g. Compute the next estimation of the DoAs using MUSIC or root-MUSIC algorithm.

h. $i=i+1$

if $\| \hat{\phi}^{(i)}-\hat{\phi}^{(i-1)} \|_2<\tau$ **then**

Stop the procedure and exit the loop

end if

end while

VI. IMPACT OF THE RESIDUAL ERROR ON THE SIGNAL AND NOISE SUBSPACES

As shown in (33), the transformation error, $\mathbf{\Delta d}_1$, will be appeared as the matrix $\mathbf{B}(\phi)$ in the covariance matrix $\mathbf{R}_c$. The IMTBR method eliminates the effect of this error iteratively. In this section, we will show that if the estimation and elimination of this error is not performed, we have a bias in the estimated DoAs.

The Eigen decomposition of the Toeplitz covariance matrix, $\mathbf{R}_c$, can be written as

$$\begin{aligned}\mathbf{R}_c &= \hat{\mathbf{E}}\hat{\mathbf{\Lambda}}\hat{\mathbf{E}}^H=\hat{\mathbf{E}}_s\hat{\mathbf{\Lambda}}_s\hat{\mathbf{E}}_s^H+\sigma^2\hat{\mathbf{E}}_\eta\hat{\mathbf{E}}_\eta^H \\ &=\left(\mathbf{E}_s+\mathbf{\Delta E}_s\right)\left(\mathbf{\Lambda}_s+\mathbf{\Delta\Lambda}_s\right)\left(\mathbf{E}_s+\mathbf{\Delta E}_s\right)^H+\sigma^2\left(\mathbf{E}_\eta+\mathbf{\Delta E}_\eta\right)\left(\mathbf{E}_\eta+\mathbf{\Delta E}_\eta\right)^H\end{aligned} \tag{38}$$

where $\hat{\mathbf{E}}_s=\mathbf{E}_s+\Delta\mathbf{E}_s$ denotes perturbed signal subspace eigenvectors, $\hat{\mathbf{\Lambda}}_s=\mathbf{\Lambda}_s+\mathbf{\Delta\Lambda}_s$ shows the eigenvalues associated with the signal subspace and $\hat{\mathbf{E}}_\eta=\mathbf{E}_\eta+\mathbf{\Delta E}_\eta$ presents perturbed noise subspace eigenvectors. The columns of the matrices $\mathbf{E}_s$, $\mathbf{E}_\eta$ and diagonal elements of the matrix $\mathbf{\Lambda}_s$ contain the true signal subspace Eigen vectors, true noise subspace Eigen vectors and true signal subspaces Eigen values, respectively. Similarly, $\mathbf{\Delta E}_s$, $\mathbf{\Delta E}_\eta$, and $\mathbf{\Delta\Lambda}_s$ contain the errors of signal subspace Eigen vectors, the noise subspace Eigen vectors and the signal subspaces Eigen values due to the effect of $\mathbf{B}(\phi)$, respectively. From (38), for $k=1,2,...,K$ the following relationships are valid:

$$\mathbf{g}^H\left(\phi_k\right)\hat{\mathbf{E}}_\eta\neq\mathbf{0} \tag{39}$$

$$\mathbf{g}^H\left(\phi_k\right)\mathbf{E}_\eta=\mathbf{0} \tag{40}$$

where $\mathbf{g}\left(\phi_k\right)$ is the k-th column of the matrix $\mathbf{G}\left(\phi\right)$. In the MUSIC algorithm, DoAs are estimated

through finding some values of ϕ which minimize the following relationship

$$\hat{f}(\phi)=\mathbf{g}^{H}(\phi)\hat{\mathbf{E}}_{\eta}\hat{\mathbf{E}}_{\eta}^{H}\mathbf{g}(\phi). \tag{41}$$

Using Eigen decomposition, we have

$$\mathbf{R}_{c}\hat{\mathbf{E}}_{\eta}=\tilde{\sigma}^{2}\hat{\mathbf{E}}_{\eta} \tag{42}$$

Substituting the $\mathbf{R}_{c}$ from (33) in (42), we have

$$\left(\mathbf{G}(\phi)\mathbf{C}\mathbf{G}^{H}(\phi)+\mathbf{B}(\phi)+\tilde{\sigma}^{2}\mathbf{I}\right)\hat{\mathbf{E}}_{\eta}=\tilde{\sigma}^{2}\hat{\mathbf{E}}_{\eta} \tag{43}$$

Considering $\hat{\mathbf{E}}_{\eta}=\mathbf{E}_{\eta}+\Delta\mathbf{E}_{\eta}$ and $\mathbf{G}^{H}(\phi)\mathbf{E}_{\eta}=\mathbf{0}$, (44) will be derived.

$$\Delta\mathbf{E}_{\eta}=-\left(\mathbf{G}(\phi)\mathbf{C}\mathbf{G}^{H}(\phi)+\mathbf{B}(\phi)\right)^{-1}\mathbf{B}(\phi)\mathbf{E}_{\eta} \tag{44}$$

The first-order expansion of $\hat{f}^{'}(\phi)$ can be used to evaluate the estimation error. If the error is considered to be small enough, the first-order expansion of $\hat{f}^{'}(\phi)$ about $\hat{\phi}_{k}$ is written as follows:

$$0=f^{'}(\hat{\phi}_{k})=\hat{f}^{'}(\phi_{k})+\hat{f}^{''}(\phi_{k})(\hat{\phi}_{k}-\phi_{k}) \tag{45}$$

From (41), the first-order derivative of $\hat{f}(\phi_{k})$ can be obtained as

$$\hat{f}^{'}(\phi_{k})=\mathbf{g}^{'H}(\phi_{k})\hat{\mathbf{E}}_{\eta}\hat{\mathbf{E}}_{\eta}^{H}\mathbf{g}(\phi_{k})+\mathbf{g}^{H}(\phi_{k})\hat{\mathbf{E}}_{\eta}\hat{\mathbf{E}}_{\eta}^{H}\mathbf{g}^{'}(\phi_{k})=2\Re\left\{\mathbf{g}^{'H}(\phi_{k})\hat{\mathbf{E}}_{\eta}\hat{\mathbf{E}}_{\eta}^{H}\mathbf{g}(\phi_{k})\right\} \tag{46}$$

where $\mathbf{g}^{'}(\phi_{k})$ is

$$\mathbf{g}^{'}(\phi_{k})=\frac{\partial\mathbf{g}(\phi_{k})}{\partial\phi_{k}}=\begin{bmatrix}0\\ je^{j\phi_{k}}\\ \vdots\\ jMe^{jM\phi_{k}}\end{bmatrix} \tag{47}$$

Considering $\hat{\mathbf{E}}_{\eta}=\mathbf{E}_{\eta}+\Delta\mathbf{E}_{\eta}$, the first-order derivative of $\hat{f}(\phi_{k})$ can be rewritten as

$$\hat{f}^{'}(\phi_{k})=2\Re\left\{\mathbf{g}^{'H}(\phi_{k})\left(\mathbf{E}_{\eta}+\Delta\mathbf{E}_{\eta}\right)\left(\mathbf{E}_{\eta}+\Delta\mathbf{E}_{\eta}\right)^{H}\mathbf{g}(\phi_{k})\right\} \tag{48}$$

From (40) and (44) and by neglecting the terms that orders higher than one, the first-order derivative of $\hat{f}(\phi_{k})$ can be derived as follows:

$$\hat{f}^{'}(\phi_{k})\approx-2\Re\left\{\mathbf{g}^{'H}(\phi_{k})\mathbf{E}_{\eta}\mathbf{E}_{\eta}^{H}\mathbf{B}^{H}(\phi)\left(\mathbf{G}(\phi)\mathbf{C}^{H}\mathbf{G}^{H}(\phi)+\mathbf{B}^{H}(\phi)\right)^{-1}\mathbf{g}(\phi_{k})\right\} \tag{49}$$

Similarly, the second order derivative would be as

$$\begin{aligned}\hat{f}^{''}(\phi_{k})=-2\Re\Bigg\{&\left(\mathbf{g}^{''H}(\phi_{k})\mathbf{E}_{\eta}\mathbf{E}_{\eta}^{H}\mathbf{B}^{H}(\phi)+\mathbf{g}^{'H}(\phi_{k})\mathbf{E}_{\eta}\mathbf{E}_{\eta}^{H}\frac{\partial\mathbf{B}^{H}(\phi)}{\partial\phi_{k}}\right)\left(\left(\mathbf{G}(\phi)\mathbf{C}^{H}\mathbf{G}^{H}(\phi)+\mathbf{B}^{H}(\phi)\right)^{-1}\mathbf{g}(\phi_{k})\right.\\&\left.+\mathbf{g}^{'H}(\phi_{k})\mathbf{E}_{\eta}\mathbf{E}_{\eta}^{H}\mathbf{B}^{H}(\phi)\left(\mathbf{D}(\phi)\mathbf{g}(\phi_{k})+\left(\mathbf{G}(\phi)\mathbf{C}^{H}\mathbf{G}^{H}(\phi)+\mathbf{B}^{H}(\phi)\right)^{-1}\mathbf{g}^{'}(\phi_{k})\right)\right)\Bigg\}\end{aligned} \tag{50}$$

where $\mathbf{g}^{''}(\phi_{k})$, $\mathbf{D}(\phi)$, $\frac{\partial\mathbf{B}(\phi)}{\partial\phi_{k}}$, are defined as (51)-(53)

$$\mathbf{g}^{"}(\phi_k)=\frac{\partial^2\mathbf{g}(\phi_k)}{\partial\phi_k^2}=\begin{bmatrix}0\\-e^{j\phi_k}\\\vdots\\-M^2e^{jM\phi_k}\end{bmatrix} \tag{51}$$

$$\mathbf{D}(\phi)=-\left(\mathbf{G}(\phi)\mathbf{C}^H\mathbf{G}^H(\phi)+\mathbf{B}^H(\phi)\right)^{-1}\left(\frac{\partial\mathbf{G}(\phi)}{\partial\phi_k}\mathbf{C}^H\mathbf{G}^H(\phi)+\mathbf{G}(\phi)\mathbf{C}^H\frac{\partial\mathbf{G}^H(\phi)}{\partial\phi_k}+\frac{\partial\mathbf{B}^H(\phi)}{\partial\phi_k}\right)\left(\mathbf{G}(\phi)\mathbf{C}^H\mathbf{G}^H(\phi)+\mathbf{B}^H(\phi)\right)^{-1} \tag{52}$$

$$\frac{\partial\mathbf{B}(\phi)}{\partial\phi_k}=\begin{bmatrix}\frac{\partial b_{M+1,M+1}(\phi)}{\partial\phi_k} & \frac{\partial b_{M+1,M+2}(\phi)}{\partial\phi_k} & \cdots & \frac{\partial b_{M+1,2M+1}(\phi)}{\partial\phi_k}\\ \frac{\partial b_{M+1,M}(\phi)}{\partial\phi_k} & \cdots & \cdots & \frac{\partial b_{M+1,2M}(\phi)}{\partial\phi_k}\\ \vdots & \vdots & \ddots & \vdots\\ \frac{\partial b_{M+1,1}(\phi)}{\partial\phi_k} & \frac{\partial b_{M+1,2}(\phi)}{\partial\phi_k} & \cdots & \frac{\partial b_{M+1,M+1}(\phi)}{\partial\phi_k}\end{bmatrix} \tag{53}$$

In (53), $\frac{\partial b_{M+1,h}(\phi)}{\partial\phi_k}$ can be defined as

$$\frac{\partial b_{M+1,h}(\phi)}{\partial\phi_k}=P\frac{\partial\Delta d_{1,M+1}(\phi_k)}{\partial\phi_k}\rho_k\sum_{q=1}^{K}\rho_q^*\tilde{a}_h^*(\phi_q)+P\frac{\partial\tilde{a}_h^*(\phi_k)}{\partial\phi_k}\rho_k^*\sum_{q=1}^{K}\rho_q\Delta d_{1,M+1}(\phi_q)+$$
$$P\left(\frac{\partial\left(\tilde{a}_{M+1}(\phi_k)+\Delta d_{1,M+1}(\phi_k)\right)}{\partial\phi_k}\right)\rho_k\sum_{q=1}^{K}\rho_q^*\Delta d_{1,h}^*(\phi_q)+P\left(\frac{\partial\Delta d_{1,h}^*(\phi_k)}{\partial\phi_k}\right)\rho_k^*\sum_{q=1}^{K}\rho_q\left(\tilde{a}_{M+1}(\phi_q)+\Delta d_{1,h}(\phi_q)\right) \tag{54}$$

Combining (49) with (50), estimation error for the k -th source is

$$\left(\hat{\phi}_k-\phi_k\right)=-\frac{\hat{f}^{'}(\phi_k)}{\hat{f}^{"}(\phi_k)} \tag{55}$$

In the next section, this bias term is derived using simulations and numerical methods.

VII. COMPUTATIONAL COMPLEXITY

In this section, the computational complexity of the proposed method is investigated based on the implementation details, which are introduced in section V. Also, we compare the complexity order of the proposed method with the previous ones, MODE-TOEP [26], Forward Backward Spatial Smoothing (FBSS) [28], and Modified UCA-ESPRIT [29].

In our proposed method, calculation of the initial beamspace vectors, $\mathbf{y}(t), t=1,...,L$, has the complexity order of $\mathcal{O}(MNL)$. The complexities of $\frac{\mathbf{J}_\zeta^{-1}}{\sqrt{N}}\hat{\mathbf{y}}(t)$ and construction of the Toeplitz structured

covariance matrix are $\mathcal{O}(ML)$. The main steps of MUSIC algorithm are calculation of noise subspace using Eigen decomposition, calculation of spatial spectrum and finding its peak values. The orders of the complexity of the first two steps of MUSIC algorithm are $\mathcal{O}(M^3)$, $\mathcal{O}(M^2)$, respectively. The complexity of the third step can be ignored, because after the first iteration, we can limit the search area of spatial spectrum around the estimated values of DoAs. For computation of $\mathbf{F}_{e_1}$ and $\mathbf{F}_{e_2}$, pseudo inverse of $N \times K$ matrix, $\mathbf{A}(\phi)$, must be calculated, which has the complexity of $\mathcal{O}(NK^2)$. The complexity order of calculation of $\tilde{\mathbf{y}}_1(t)$ and $\tilde{\mathbf{y}}_2(t)$ for all snapshots is $\mathcal{O}(MNL)$.

In MODE-TOEP method, after the application of BT and construction of Toeplitz covariance matrix, MUSIC algorithm is applied to find DoAs. In this method, the residual error of BT is not compensated. FBSS is one of the most important techniques in DoA estimation of coherent sources [28]. In this algorithm after the application of BT, the main array (in our case VULA array) is divided into multiple overlapping sub-arrays. In each sub-array, the covariance matrix will be estimated. The final forward backward smoothed covariance matrix is given by [28]

$$\mathbf{R}_{fb} = \frac{1}{2D}\sum_{l=1}^{D}\mathbf{H}_l^T[\mathbf{J}_\zeta^{-1}\mathbf{F}_e^H\mathbf{R}_{\mathbf{x}}\mathbf{F}_e\mathbf{J}_\zeta^{-1} + \tilde{\mathbf{I}}_{2M+1}(\mathbf{J}_\zeta^{-1}\mathbf{F}_e^H\mathbf{R}_{\mathbf{x}}\mathbf{F}_e\mathbf{J}_\zeta^{-1})^*\tilde{\mathbf{I}}_{2M+1}]\mathbf{H}_l \tag{56}$$

where $\mathbf{H}_l = \left[\mathbf{e}_l, \mathbf{e}_{l+1}, ..., \mathbf{e}_{l+L_0-1}\right]$ with $\mathbf{e}_l$ denoting the l-th column of the identity matrix of size $2M+1$, D is the number of sub-arrays, and $L_0 = 2M - D + 2$ is the sub-array length.

Both FBSS and MODE-TOEP methods are applied after BT, thus they have the complexity order of $\mathcal{O}(MNL) + \mathcal{O}(ML)$ for calculation of $\mathbf{z}(t), t = 1, 2, ..., L$ using (23) and (29). The main difference between FBSS and MODE-TOEP is type of construction of covariance matrix and its dimension. Dimension of covariance matrix in FBSS method is $L_0 \times L_0$ while it is $(M+1)\times(M+1)$ in MODE-TOEP and IMTBR methods. Based on (56), the complexity order of calculation of covariance matrix in FBSS method is $\mathcal{O}(DN^2L)$. Also, the complexity of MUSIC algorithm for FBSS method is $\mathcal{O}(L_0^3) + \mathcal{O}(L_0^2)$. Therefore, the total complexity order of FBSS is $\mathcal{O}(MNL) + \mathcal{O}(ML) + \mathcal{O}(DN^2L) + \mathcal{O}(L_0^3) + \mathcal{O}(L_0^2)$.

Similar to FBSS and MODE-TOEP methods, Modified UCA-ESPRIT is applied after BT. Complexity order of this step is $\mathcal{O}(MNL) + \mathcal{O}(ML)$. In the second step, a Hermitian Toeplitz covariance matrix can be reconstructed from the obtained vectors with complexity of $\mathcal{O}(M^2L)$. Finally, the DoAs are estimated by applying ESPRIT method on the obtained covariance matrix, where its complexity is $\mathcal{O}(M^3)$. Table II shows the complexity order of IMTBR, MODE-TOEP, FBSS and Modified UCA-ESPRIT algorithms.

Table II. Comparison of computational complexity.

Algorithms	Complexity order	Dominant terms
IMTBR-MUSIC	$\mathcal{O}(MNL)+\mathcal{O}(N_{itr}ML)+\mathcal{O}(N_{itr}ML)+\mathcal{O}(N_{itr}M^3)+\mathcal{O}(N_{itr}M^2)$ $+\mathcal{O}(N_{itr}NK^2)+\mathcal{O}(N_{itr}NK^2)+\mathcal{O}(N_{itr}MNL)+\mathcal{O}(N_{itr}MNL)$	$\mathcal{O}(N_{itr}MNL)$
MODE-TOEP	$\mathcal{O}(MNL)+\mathcal{O}(ML)+\mathcal{O}(ML)+\mathcal{O}(M^3)+\mathcal{O}(M^2)$	$\mathcal{O}(MNL)$
FBSS	$\mathcal{O}(MNL)+\mathcal{O}(ML)+\mathcal{O}(DN^2L)+\mathcal{O}(L_0^3)+\mathcal{O}(L_0^2)$	$\mathcal{O}(DN^2L)$
Modified UCA-ESPRIT	$\mathcal{O}(MNL)+\mathcal{O}(ML)+\mathcal{O}(M^3)$	$\mathcal{O}(MNL)$

Since L is larger than N, M, K, L_0 and D, the dominant terms of complexity order of IMTBR-MUSIC, MODE-TOEP, FBSS, and Modified UCA-ESPRIT algorithms are $\mathcal{O}\left(N_{itr}MNL\right)$, $\mathcal{O}\left(MNL\right)$, $\mathcal{O}\left(DN^2L\right)$, $\mathcal{O}\left(MNL\right)$, respectively. Since $M > N$ and D is of order of N_{itr} (both are assumed to be 3 in simulations), the complexity of IMTBR is less than FBSS and higher than MODE-TOEP and Modified UCA-ESPRIT. Simulation results in next section shows that IMTBR with only three iterations can achieve better performance with respect to estimation error in comparison to FBSS, MODE-TOEP and Modified UCA-ESPRIT methods. Thus, the cost of higher complexity in comparison to MODE-TOEP and Modified UCA-ESPRIT methods is reasonable against this profit.

VIII. SIMULATION RESULTS

In this section, the performance of IMTBR method will be evaluated for the DoA estimation of coherent sources. Also, the performance of IMTBR method is compared with the previous ones, MODE-TOEP [26], FBSS [28] and Modified UCA-ESPRIT [29]. Depending on the application of MUSIC or root-MUSIC algorithm in each iteration (see Fig. 2), the proposed algorithm is called IMTBR-MUSIC and IMTBR-root MUSIC, respectively. Root Mean Square Error (RMSE) is used as a performance metric to evaluate the accuracy of DoA estimation methods and it is defined as follows [30]:

$$\text{RMSE}=\sqrt{\frac{1}{N_{MC}\times K}\sum_{k=1}^{K}\sum_{e=1}^{N_{MC}}\left(\phi_k-\hat{\phi}_{k,e}\right)^2} \tag{57}$$

where $\hat{\phi}_{k,e}$ is the estimation of ϕ_k in the e-th Monte-Carlo trial. The number of Monte-Carlo trials is assumed to be $N_{MC}=1000$.

Cramér-Rao Bound (CRB) is an upper bound on the performance (lower bound on the error variance) of any unbiased estimation method. CRB for DoA estimation of coherent sources is obtained as [31]

$$\text{CRB}_{\phi}=\frac{1}{2L\sigma^2}\left[\Re\left\{\mathbf{D}^H(\mathbf{I}_N-\mathbf{A}(\phi)(\mathbf{A}(\phi)^H\mathbf{A}(\phi))^{-1}\mathbf{A}(\phi)^H)\mathbf{D}\right\}\odot\left(\mathbf{R}_{\mathbf{s}}\mathbf{A}(\phi)^H\mathbf{R}_{\mathbf{x}}^{-1}\mathbf{A}(\phi)\mathbf{R}_{\mathbf{s}}\right)^T\right]^{-1} \tag{58}$$

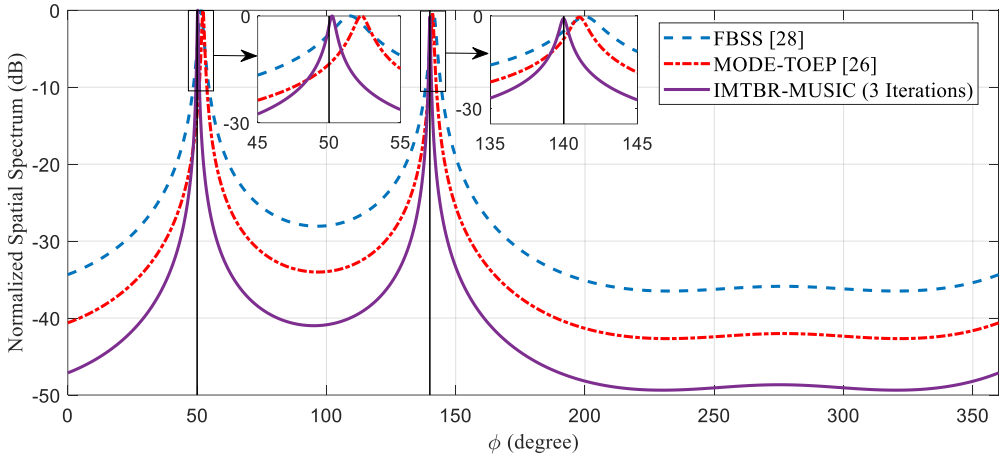

Fig. 3. Comparison between the spatial spectrum of different algorithms: IMTBR-MUSIC, MODE-TOEP, and FBSS with $L = 500$ and SNR = 10dB for two coherent sources with angles $\phi_1 = 50^\circ$ and $\phi_2 = 140^\circ$.

where $\mathbf{D} = \left[\frac{d\mathbf{a}(\phi_1)}{d\phi_1}, \frac{d\mathbf{a}(\phi_2)}{d\phi_2}, ..., \frac{d\mathbf{a}(\phi_K)}{d\phi_K} \right]$, $\mathbf{R}_\mathbf{s} = E\left\{\mathbf{s}(t)\mathbf{s}^H(t)\right\}$, and $\mathbf{R}_\mathbf{x} = E\left\{\mathbf{x}(t)\mathbf{x}^H(t)\right\}$. The (k,k)-th entry of the matrix CRB_ϕ is equal to CRB of the DoA estimation error of the k-th source. Average CRB is obtained by taking average of the CRB of K sources. For two sources with powers of $\mathbf{P} = \left[P_1\ P_2\right]^T$ and correlation coefficient of $\rho_{1,2}$, the above-mentioned matrices can be calculated as

$$\mathbf{R}_\mathbf{s} = \begin{bmatrix} P_1 & \rho_{1,2}\sqrt{P_1P_2} \\ \rho_{1,2}\sqrt{P_1P_2} & P_2 \end{bmatrix} \tag{59}$$

$$\mathbf{R}_\mathbf{x} = \left[\mathbf{a}(\phi_1)\ \mathbf{a}(\phi_2)\right] \begin{bmatrix} P_1 & \rho_{1,2}\sqrt{P_1P_2} \\ \rho_{1,2}\sqrt{P_1P_2} & P_2 \end{bmatrix} \begin{bmatrix} \mathbf{a}^H(\phi_1) \\ \mathbf{a}^H(\phi_2) \end{bmatrix} + \sigma^2\mathbf{I}_N \tag{60}$$

In the first set of simulations, it is assumed that there are two coherent narrowband signals with azimuths $\phi_1 = 50^\circ$, $\phi_2 = 140^\circ$, a UCA with radius $r = Mc/2\pi f$, $f = 1GHz$ and $N = 8$ antennas. Also, by assuming $M = 3$, the virtual array contains 7 antennas. In IMTBR method, it has been assumed that the maximum number of iterations is $N_{itr} = 3$, while the stopping threshold in Algorithm 1 is chosen $\tau = 10^{-2}$.

Fig. 3 shows the spatial spectrums of FBSS, MODE-TOEP, and IMTBR-MUSIC after 3 iterations at SNR = 10dB and $L = 500$. It is observed that the peaks of spatial spectrum in IMTBR algorithm are more accurate and sharper than the other ones.

Fig. 4 depicts the RMSE of proposed algorithm with different number of iterations for two coherent sources. Increasing SNR will improve the performance of IMTBR algorithm in different iterations. As shown in this figure, the estimation accuracy of proposed algorithm in different iterations using MUSIC or root-MUSIC is almost the same. Simulation results show that the proposed IMTBR algorithm converges after 3 iterations and its performance is very close to CRB.

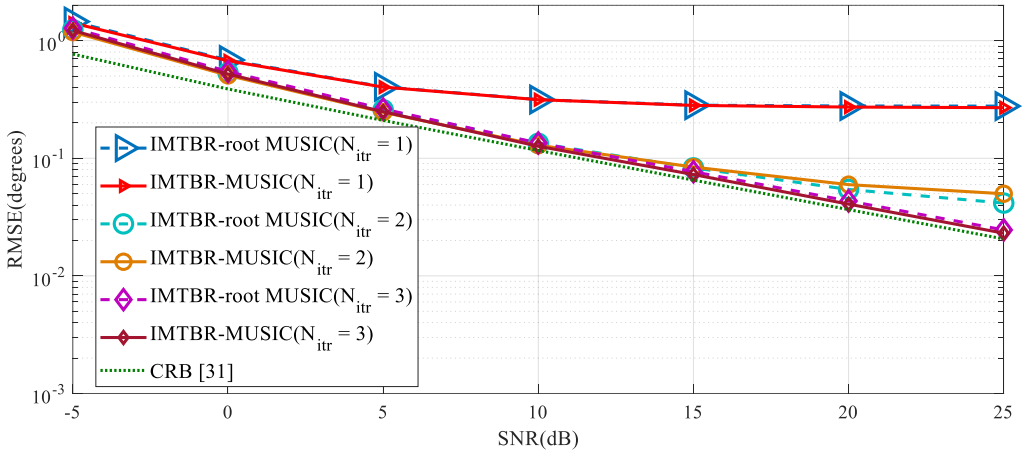

Fig. 4. RMSE of proposed IMTBR method versus SNR using different iterations for two coherent sources with $\phi_1 = 50^\circ$ and $\phi_2 = 140^\circ$, $L = 500$ and stopping threshold $\tau = 10^{-2}$.

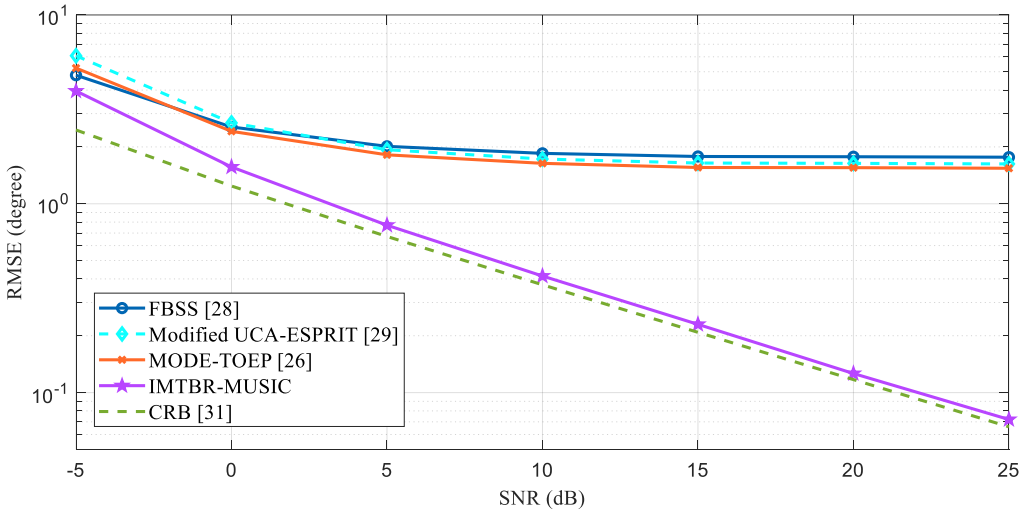

Fig. 5. Comparison between the RMSE of FBSS, MODE-TOEP and IMTBR methods versus SNR for two coherent sources with $\phi_1 = 50^\circ$, $\phi_2 = 140^\circ$, $L = 50$, stopping threshold for IMTBR-MUSIC $\tau = 10^{-2}$ and $N_{itr} = 3$.

Fig. 5 shows the RMSE of IMTBR method for DoA estimation of two coherent signals in comparison to FBSS and MODE-TOEP algorithms. The results indicate that increasing SNR will improve the performance of algorithms. It can be observed that the RMSE of proposed algorithm is lower than that of MODE-TOEP and FBSS. In MODE-TOEP and FBSS algorithms, the residual error of BT is not compensated. Hence, performance of these algorithms is saturated when SNR is increased, which is due to the BT residual error, while IMTBR does not suffer from error saturation.

In Fig. 6, the RMSE of IMTBR has been compared with MODE-TOEP and FBSS algorithms for the different number of snapshots, L. In this figure, the SNR is equal to 0dB. It is observed that the IMTBR has a better performance than that of MODE-TOEP and FBSS algorithms. Although by increasing the number of snapshots we achieve a better approximation of covariance matrix, but the RMSE of MODE-TOEP and FBSS algorithms is saturated due to the residual error of BT.

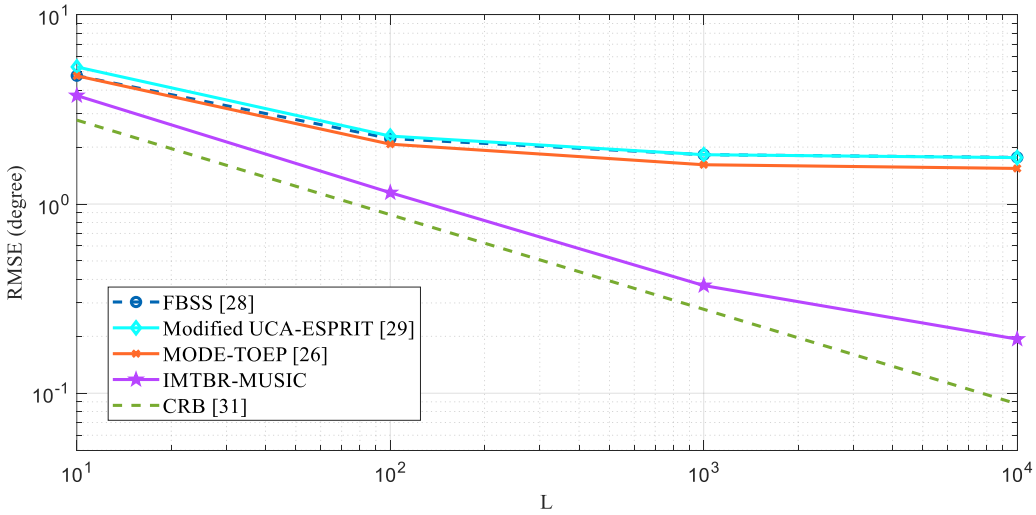

Fig. 6. Comparison between the RMSE of FBSS, MODE-TOEP and IMTBR methods versus number of snapshots, L, for two coherent sources with $\phi_1 = 50^\circ$ and $\phi_2 = 140^\circ$, stopping threshold for IMTBR-MUSIC $\tau = 10^{-2}$ and $N_{itr} = 3$ at SNR = 0dB.

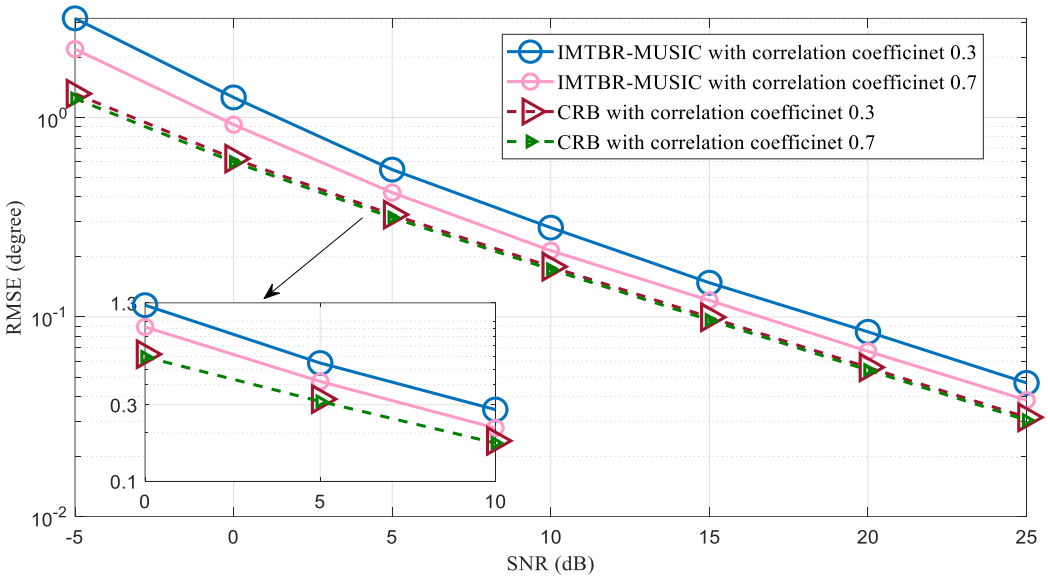

Fig. 7. RMSE versus SNR for two partially correlated sources with different correlation coefficients, $\phi_1 = 50^\circ$, $\phi_2 = 140^\circ$, $L = 256$, stopping threshold for IMTBR-MUSIC $\tau = 10^{-2}$ and $N_{itr} = 3$.

In Fig. 7, two sources with different correlation coefficients are assumed and the RMSE of proposed algorithm is compared with CRB. It is observed that the proposed algorithm also works well (close to CRB) for the cases where the signals are partially correlated.

In Fig. 8, the effect of the residual error on the performance of MODE-TOEP method is illustrated. In this figure, we have shown the bias of DoA estimation using simulation results and then it has been calculated using the results of section VI. As can be seen, first order approximation which is derived in section VI for the bias of DoA estimation of coherent sources using BT is completely matched with simulations. It is noteworthy that when the SNR increases, the RMSE of estimation decreases.

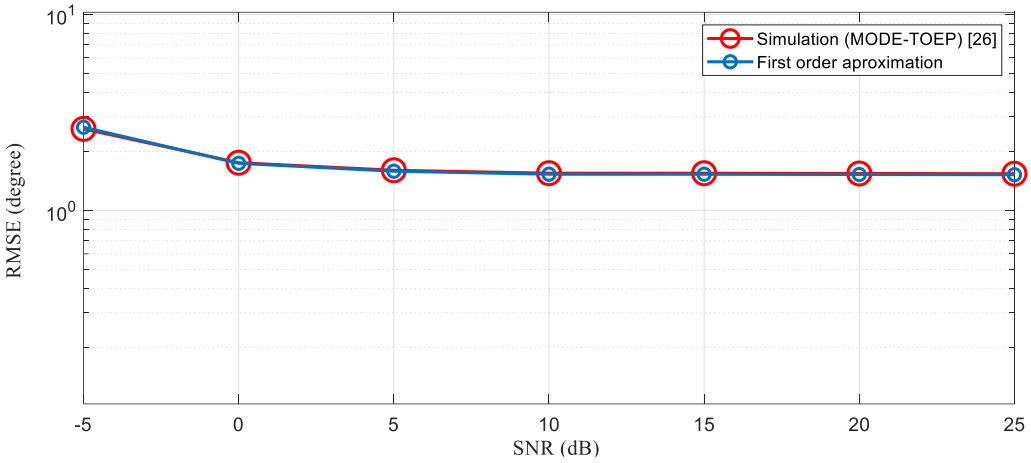

Fig. 8. Comparison between the RMSE of MODE-TOEP method using MUSIC algorithm and the first-order approximation of the bias for two coherent sources with azimuths $\phi_1 = 50^\circ$, $\phi_2 = 140^\circ$ and $L = 256$.

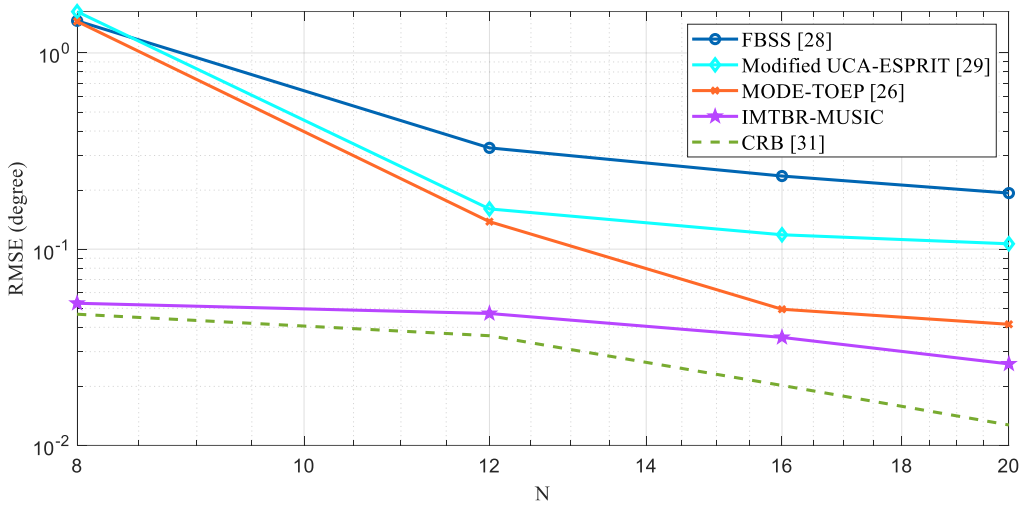

Fig. 9. Comparison between the RMSE of Modified UCA-ESPRIT, FBSS, MODE-TOEP and IMTBR methods versus different number of antennas, N, for two coherent sources with $\phi_1 = 50^\circ$, $\phi_2 = 140^\circ$, $L = 100$, SNR = 25dB, stopping threshold for IMTBR-MUSIC $\tau = 10^{-2}$ and $N_{itr} = 3$.

However, a bias term appears as an error floor.

In the next simulation, RMSE of different methods versus number of UCA antennas, N, is evaluated. Similar to the previous simulations, two coherent sources with DoAs $\phi_1 = 50^\circ$, $\phi_2 = 140^\circ$ are considered. As shown in Fig. 9, RMSE of different methods is decreased by increasing the number of antennas. The obtained results show that the IMTBR method has lower RMSE in comparison with the Modified UCA-ESPRIT, FBSS and MODE-TEOP methods.

Following, we consider a case that the number of coherent sources is $K = 3$ with angles $\phi_1 = 50^\circ$, $\phi_2 = 140^\circ$, and $\phi_3 = 250^\circ$. The RMSE of different methods are compared in Fig. 10. As can be observed from this figure, by increasing the SNR of received vectors, the RMSE of IMTBR method is decreased, whereas, the other methods have a fixed.

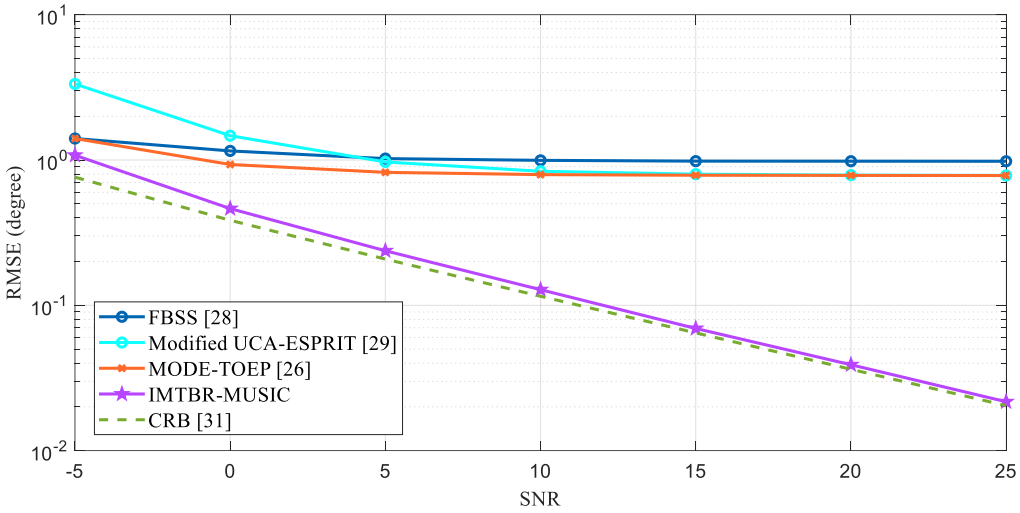

Fig. 10. Comparison between the RMSE of Modified UCA-ESPRIT, FBSS, MODE-TOEP and IMTBR methods versus SNR, for three coherent sources with $\phi_1 = 50^\circ$, $\phi_2 = 140^\circ$, $\phi_2 = 250^\circ$, $L = 1000$, stopping threshold for IMTBR-MUSIC $\tau = 10^{-2}$ and $N_{itr} = 3$.

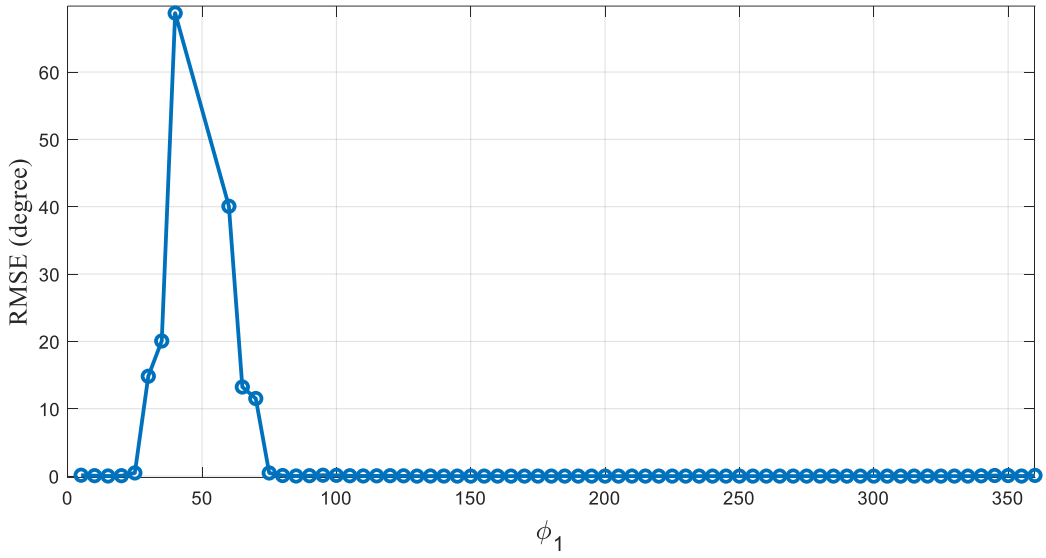

Fig. 11. RMSE of IMTBR method for $K = 2$ coherent sources at SNR=50dB, $L = 1000$, $\phi_1 = 50^\circ$ and $\phi_2 = [5,360]^\circ$, $N = 8$, $M = 3$, stopping threshold for IMTBR-MUSIC $\tau = 10^{-2}$, and $N_{itr} = 3$.

In the last simulation, the effect of closely spaced sources is investigated. In this simulation, two coherent sources are considered, wherein the first source is fixed with $\phi_1 = 50^\circ$, while the angle of the second source is varied in $\phi_2 = [5,360]^\circ$ with 5-degree steps. Figure 11 shows the RMSE of IMTBR method for $L = 1000$ and SNR = 50dB. As can be seen, when two sources are not closely spaced, the RMSE of IMTBR method tends to zero. However, by decreasing the difference of DoAs, the angle of one of sources will be estimated with high error.

IX. CONCLUSION

In this paper, a new algorithm for DoA estimation of coherent sources with the UCA is proposed. At the first step the steering vectors of UCA is mapped to the steering vector of an array with the Vandermonde structure, using the beamspace transformation. This transformation method causes an additional error in DoA estimation, which is a function of direction of emitters. To reduce the RMSE of DoA estimation of the coherent sources in UCA, an iterative algorithm was proposed. The MODE-TOEP algorithm was used to overcome the source correlation problem and the MUSIC algorithm was used for DoA estimation. In this algorithm, the dominant error term is reduced using two beamformers and the first-order approximation of bias for the DoA estimation of coherent sources was derived. Finally, the simulation results showed that the proposed algorithm has lower RMSE compared to the conventional algorithms and its performance is very close to CRB.

REFERENCES

[1] N. Ahmed, H. Wang, M. A. Z. Raja, W. Ali, F. Zaman, W. U. Khan, and Y. He "Performance analysis of efficient computing techniques for direction of arrival estimation of underwater multi targets," *IEEE Access*, vol. 9, pp. 33284-33298, Feb. 2021.

[2] I. Aboumahmoud, A. Muqaibel, M. Alhassoun, and S. Alawsh, "A review of sparse sensor arrays for two-dimensional direction-of-arrival astimation," *IEEE Access*, vol. 9, pp. 92999-93017, June 2021.

[3] Z. Yang, J. Li, P. Stoica, and L. Xie, "Sparse methods for direction-of-arrival estimation," Academic Press Library in Signal Processing, vol. 7, R. Chellappa and S. Theodoridis, Eds., April 2018, pp. 509–581.

[4] Y. Fang, S. Zhu, Y. Gao, L. Lan, C. Zeng, and Z. Liu, "Direction-of-arrival estimation of coherent signals for uniform linear antenna arrays with mutual coupling in unknown nonuniform noise," *IEEE Trans. on Vehicular Technology*, vol. 71, no. 2, pp. 1656-1668, Feb. 2022.

[5] M. W. T. S. Chowdhury, and M. Mastora, "Performance analysis of MUSIC algorithm for DOA estimation with varying ULA parameters," 23*rd Intern. Conf. on Computer and Information Technology (ICCIT)*, April 2021, pp. 1-5.

[6] M. Bensalem and O. Barkat, "DOA estimation of linear dipole array with known mutual coupling based on ESPRIT and MUSIC," *Radio Science*, vol. 57, no. 2, pp. 1-15, Jan. 2022.

[7] S. Li and B. Lin, "On spatial smoothing for direction-of-arrival estimation of coherent signals in impulsive noise," *IEEE Advanced Information Technology, Electronic and Automation Control Conference (IAEAC)*, March 2016, pp. 339-343.

[8] W. Zhang, Y. Han, M. Jin, and X. S. Li, "An Improved ESPRIT-Like Algorithm for Coherent Signals DoA Estimation," *IEEE Communications Letters*, vol. 24, no. 2, pp. 339-343, Feb. 2020.

[9] S. U. Pillai and B. H. Kwon, "Forward/backward spatial smoothing techniques for coherent signal identification," *IEEE Trans. on Acoustics, Speech, and Signal Processing*, vol. 37, no. 1, pp. 8-15, Jan. 1989.

[10] J. Pan, M. Sun, Y. Wang, X. Zhang, J. Li, and B. Jin, "Simplified spatial smoothing for DoA estimation of coherent signals," *IEEE Trans. on Circuits and Systems II*: *Express Briefs*, vol. 1, pp. 1-5, Oct. 2022.

[11] W. Zhang, Y. Han, M. Jin, and X. Qiao, "Multiple-Toeplitz Matrices Reconstruction Algorithm for DoA Estimation of Coherent Signals," *IEEE Access*, vol. 7, pp. 49504-49512, April 2019.

[12] W. Zhang and X. -s. Li, "A Modified MODE-TOEP Algorithm for Estimating Coherent Signals DoA on Uniform Circular Array," *2020 Intern. Conf. on Computer Engineering and Application (ICCEA)*, March 2020, pp. 525-528.

[13] F. Liu, J. Wang, C. Sun, and R. Du, "Spatial differencing method for DOA estimation under the coexistence of both uncorrelated and coherent signals," *IEEE Trans. on Antennas and Propagation*, vol. 60, no. 4, pp. 2052-2062, Jan. 2012.

[14] M. A. Parian, G. Sedigheh, "M- $\ell_{2,1}$ MUSIC algorithm for DoA estimation of coherent sources," *IET Signal Processing*, vol. 11, no. 4, pp. 429-436, June 2017.

[15] B. Qi, "DoA estimation of the coherent signals using beamspace matrix reconstruction," *Signal Processing*, vol. 191, pp. 1-15, Feb. 2022.

[16] T. Liang, M. Zhu, and F. Pan, "A DoA estimation method for uniform circular array based on virtual interpolation and subarray rotation," *IEEE Access*, vol. 9, pp. 116760-116767, Aug. 2021.

[17] P. Hyberg, M. Jansson, and B. Ottersten, "Array interpolation and bias reduction," *IEEE Trans. on Signal Processing*, vol. 52, no. 10, pp. 2711-2720, Sept. 2004.

[18] M. Y. Cao, L. Huang, W. X. Xie, and H. C. So, "Interpolation array technique for direction finding via Taylor series fitting," *IEEE China Summit and Intern. Conf. on Signal and Information Processing (ChinaSIP)*, Sept. 2015, pp. 736-740.

[19] R. M. Shubair, A. S. Goian, M. I. AlHajri, and A. R. Kulaib, "A new technique for UCA-based DoA estimation of coherent signals," *16th Mediterranean Microwave Symposium (MMS)*, January 2016, pp. 1-3.

[20] F. Belloni and V. Koivunen, "Beamspace transform for UCA: error analysis and bias reduction," *IEEE Trans. on Signal Processing*, vol. 54, no. 8, pp. 3078-3089, July 2006.

[21] F. Belloni, A. Richter, and V. Koivunen, "DoA estimation via manifold separation for arbitrary array structures," *IEEE Trans. on Signal Processing*, vol. 55, no. 10, pp. 4800-4810, Sept. 2007.

[22] G. Hua, J. D. Wu, X. -C. Zhu, H. -X. Zhou, and W. Hong, "Efficient two dimensional direction finding via auxiliary-variable manifold separation technique for arbitrary array structure," *IEEE Intern. Conf. on Communiction Problem-solving*, March 2015, pp. 532-537.

[23] B. Friedlander, "The root-MUSIC algorithm for direction finding with interpolated arrays," *Signal Processing*, vol. 30, no. 1, pp. 15-29, Jan. 1993.

[24] F. Belloni, A. Richter, and V. Koivunen, "DoA estimation via manifold separation for arbitrary array structures," *IEEE Trans. on Signal Processing*, vol. 55, no. 10, pp. 4800-4810, Sept 2007.

[25] S. Li and H. Chen, "A novel method of DoA estimation on sparse uniform circular array," *CIE Intern. Conf. on Radar (RADAR)*, Oct. 2017, pp. 1-4.

[26] G. Shuyan, C. Hui, W. Yongliang, and M. Cangzhen, "A novel algorithm for estimating DoA of coherent signals on uniform circular array," CIE *Intern, Conf. on Radar*, April 2007, pp. 1-4.

[27] W. Tao, Y. Li-sheng, L. Jian-mei, and Y. Shi-zhong, "A modified MUSIC to estimate DoA of the coherent narrowband sources based on UCA," *Intern. Conf. on Communication Technology*, April 2007, pp. 1-4.

[28] K. Maheswara Reddy and V. U. Reddy, "Analysis of spatial smoothing with uniform circular arrays," *IEEE Trans. on Signal Processing*, vol. 47, no. 6, pp. 1726-1730, 1999.

[29] K. A. Jabr, H. M. Kwon, and N. Tayem, "Modified UCA-ESPRIT for Estimating DOA of Coherent Signals using One Snapshot," *IEEE Vehicular Technology Conf.*, May 2008, pp. 290-293.

[30] P. Li, J. Li, and G. Zhao, "Low complexity DoA estimation for massive UCA with single snapshot," *Journal of Systems Engineering and Electronics*, vol. 33, no. 1, pp. 22-27, Feb. 2022.

[31] F. Haddadi, M. M. Nayebi, and M. R. Aref, "Direction-of-arrival estimation for temporally correlated narrowband signals," *IEEE Trans. on Signal Processing*, vol. 57, no. 2, pp. 600-609, Feb. 2009.